© EARSeL and Warsaw University, Warsaw 2005. *Proceedings of 4th EARSeL Workshop on Imaging Spectroscopy. New quality in environmental studies*. Zagajewski B., Sobczak M., Wrzesień M., (eds)

A NEW MODEL-DRIVEN CORRECTION FACTOR FOR BRDF EFFECTS IN HRS DATA

Tal Feingersh[1], Wouter Dorigo[2], Rudolf Richter[2], Eyal Ben-Dor[1]

1. University of Tel-Aviv, Department of Geography, Tel-Aviv, Israel; ftal@post.tau.ac.il
2. German Aerospace Center (DLR), Remote Sensing Data Center (DFD), Wessling, Germany; wouter.dorigo@dlr.de

ABSTRACT

Interpretation of hyperspectral remotely sensed (HRS) imagery can be degraded by bi-directional reflectance distribution function (BRDF) effects that contribute an unknown amount of error to reflectance values. In this work we test a new empirical approach, using in-flight records concerning sensor and sun geometry at the time of acquisition, and laboratory BRDF measurements of selected land-cover classes from the new Israeli Goniometric Facility (IGF) at the remote sensing laboratory, Tel-Aviv University. BRDF datasets are then nadir-normalized (i.e. transformed to anisotropy), spectrally resampled to the required sensor and inverted to form correction vectors for the real imagery. These correction vectors are finally applied only to class-specific pixels of interest. We demonstrate this application for a non-georeferenced CASI image and four georeferenced HyMAP images and discuss results. The CASI data preliminary average anisotropy reaches ±20% and corrects down to ±5%. Its RMSE values are reduced by about 40-70%. HyMAP data Uses the same model and reduces average pre-correction ANIF by 25-50%, depending on wavelength.

Since angular information about the sensor is the base for this correction, natural variability of the corrected land-cover classes is maintained. Therefore this method allows a class-specific BRDF correction that improves interpretation capability and quantitative analysis.

INTRODUCTION

Bi-directional reflectance distribution function (BRDF) effects in hyperspectral remotely sensed (HRS) data contribute an unknown amount of error to interpretation efforts. Accuracies of land cover classifications are affected, as well as quantitative estimates of physical parameters of land-cover classes (e.g. vegetation and mineral indices, energy fluxes etc.). Previous works calibrate BRDF in HRS data by in situ measurements (i), use theoretical models for correction of these effects (ii,iii), or normalize mean column reflectance to nadir mean reflectance prior to geometric registration (iv). We suggest a new correction approach based on a set of laboratory BRDF measurements conducted at the Israel Goniometric Facility (IGF) recently built at the Remote Sensing Laboratory, at the University of Tel-Aviv (RSL-TAU).

Radiometric quantities

To understand the exact radiometric quantities that the IGF produces we relate to common values as starting points. With the intention of applying BRDF datasets to real imagery we normalize radiance differences between the image at the time of acquisition and the data in the laboratory. Reflectance, being the reflected energy flux divided by the incoming energy flux is a measure free of those differences. It relates to a set of reflected energy normalized to a full hemispherical set of directions. Following the standard definition of BRDF by Nicodemus (v) we have

$$BRDF(\varphi_i, \theta_i; \varphi_r, \theta_r; \lambda) = L(\varphi_i, \theta_i; \varphi_r, \theta_r; \lambda) / (L(\varphi_i, \theta_i; \lambda) \cdot \sin\theta_i \cdot dw) \quad (1)$$

Where

BRDF(φ_i,θ_i; φ_r,θ_r; λ) is the bi-directional reflectance distribution function for irradiance coming from azimuth and elevation direction φ_i and θ_i respectively and reflected to azimuth and elevation direction φ_r and θ_r respectively, at wavelength λ,

$L(\varphi_i,\theta_i; \varphi_r,\theta_r; \lambda)$ is the reflected radiance [W m^{-2} sr^{-1}], and

$L(\varphi_i,\theta_i; \lambda)\cdot\sin\theta_i\cdot dw$ is the incoming radiance [W m^{-2}] from solid angle dw and elevation angle θi.

Since we do not actually measure irradiance from within an incoming cone, we estimate it by measuring radiance reflected from a standard Lambertian white reference plate and use a bi-directional reflectance factor (BRF) instead (vi):

$$BRF(\varphi_i,\theta_i;\ \varphi_r,\theta_r;\ \lambda)=L(\varphi_i,\theta_i;\ \varphi_r,\theta_r;\ \lambda)\ /\ L_{ref}(\varphi_i,\theta_i;\ \varphi_r,\theta_r;\ \lambda) \quad (2)$$

BRF by itself does not reveal much when examining spectra from varying sensor positions. To emphasize position-related BRF differences (Anisotropy) we divide each BRF measurement by the nadir measurement (BRF_N) and use this anisotropy factor (ANIF) as a starting point for BRDF correction:

$$ANIF(\varphi_i,\theta_i\ ;\ \varphi_r,\theta_r\ ;\ \lambda)=BRF(\varphi_i,\theta_i\ ;\ \varphi_r,\theta_r\ ;\ \lambda)\ /\ BRF_N(\varphi_i,\theta_i\ ;\ \varphi,\theta_N\ ;\ \lambda) \quad (3)$$

Adjustment of ANIF data to field conditions

The pre-processed anisotropy from the IGF is of high spectral resolution (1nm) and a relatively low angular sampling resolution (5°). In real airborne imagery spectral resolution is usually worse than that of the IGF, but the angular resolution is better. In addition, sun position (φ_i,θ_i) can fall between illumination positions that were used with the IGF. Therefore the correction process requires adjustments of the lab dataset to the conditions at the field at the time of acquisition (i.e. sensor geometry (FOV, number of samples) flight direction (heading) and sun position (φ_i,θ_i). In the case of non-geocoded imagery, absolute φ_r and θ_r (i.e. sensor position) are computed from these data on a pixel basis. In this case, the nadir point is considered to be the middle (central) column of the image, mean heading is used for extraction of sensor azimuth position (φ_r) and sensor geometry for its elevation position (θ_r). Moreover, we assume that the terrain is flat and that aircraft roll motion has a negligible effect in the image. If this is clearly not the case then results will be poor. However in most cases an in-flight navigation file is available and these sensor position data can be reconstructed per pixel and provided along with the image itself as a "scan angle file" (e.g. sensor data processed with PARGE software, vii).

Having acquired the necessary information above, we can start running the model for BRDF correction. Assuming that the influence of illumination elevation (θ_i) on observed BRF's is changing linearly, we start by interpolating two BRF datasets that were measured with illumination elevation (θ_i) lower (a) and higher (b) than that of the sun at the time of acquisition. Weights are inversely proportional to the angular distance between the IGF data θ_i and sun θ_i such that

$$BRDF(\varphi_i,\theta_{sun}) = \frac{\left|\theta_{sun}-\theta_{i,b}\right|}{\theta_{i,b}-\theta_{i,a}}\cdot BRDF(\varphi_i,\theta_a) + \frac{\left|\theta_{sun}-\theta_{i,a}\right|}{\theta_{i,b}-\theta_{i,a}}\cdot BRDF(\varphi_i,\theta_b) \quad (4)$$

To adjust the interpolated BRF to the sun's azimuth angle we can simply shift the data's original φ_i (90°) to the sun's φ_i. This is possible since the BRF in its rectangular form is a projection of a circular set of measurements along its φ_r dimension. Finally we resample spectrally the BRDF dataset to the spectral resolution of the image to be corrected.

Suppression of anisotropy

The scan angle file layers (φ_r, θ_r) provide the necessary subscripts that are needed for the interpolation of ANIF values from the BRDF dataset. This Interpolation is bilinear, and the result is an ANIF image, per band, corresponding to the real image. Since the IGF data is generally covering angular sensor positions within a wide range ($\varphi_{2\pi}$, $\theta_{20°...90°}$) most sensors are expected to fall within the angular limits of the model. The overall workflow of the correction method is outlined in figure 1.

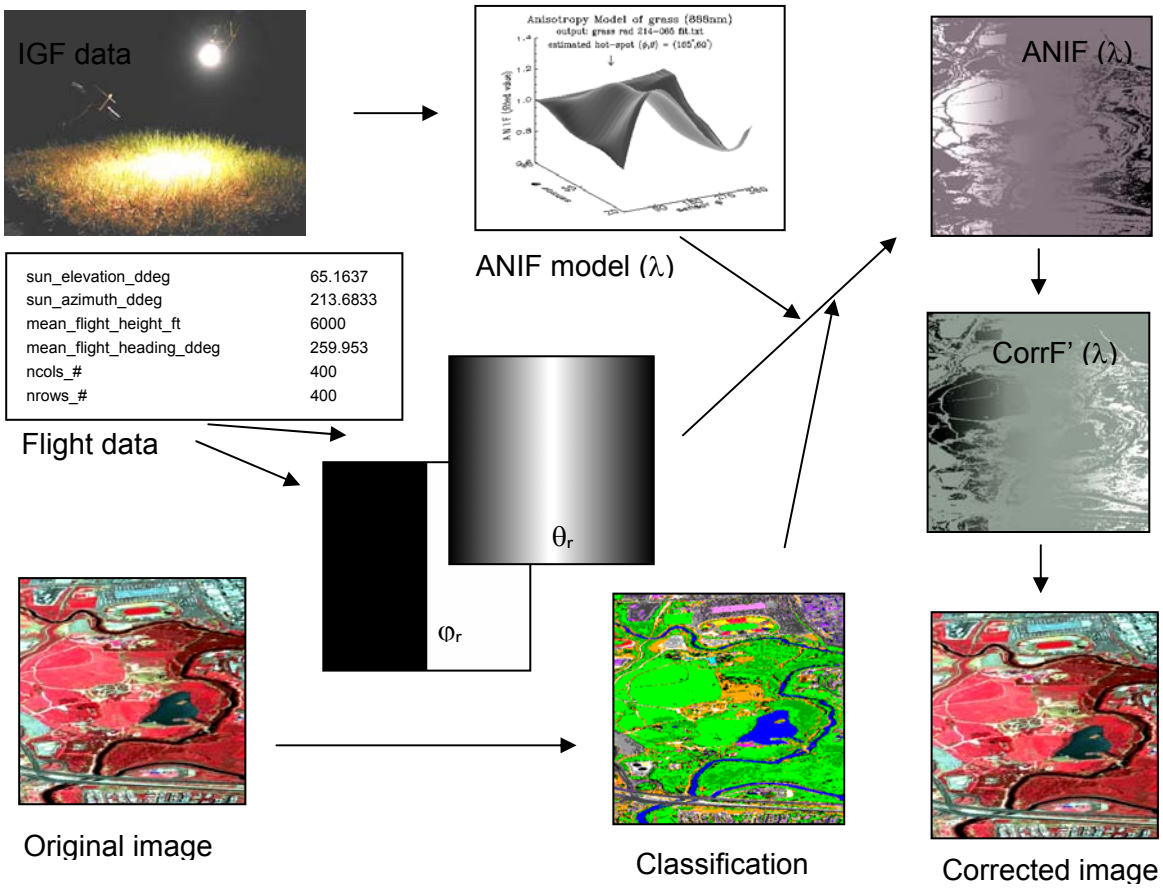

Figure 1. Workflow of the IGF-based BRDF correction of airborne imagery. BRDF measurements and flight scan angle information are merged together per pixel, to extract ANIF and CorrF values per pixel, per band (See text for a full discussion).

Correction factors (CorrF) are supposed to normalize anisotropy factors, which are in turn nadir-normalized reflectance measurements. Therefore an ANIF for a nadir measurement (θ_N) is equal to unity as well as its correction factor. An inversion of ANIF produces

$$CorrF(\varphi_i, \theta_i; \varphi_r, \theta_r; \lambda) = ANIF(\varphi_i, \theta_i; \varphi_r, \theta_N; \lambda) / ANIF(\varphi_i, \theta_i; \varphi_r, \theta_r; \lambda) = 1 / ANIF(\varphi_i, \theta_i; \varphi_r, \theta_r; \lambda) \quad (5)$$

which means that a reflectance value higher than the nadir value (and therefore having an ANIF grater than 1) will be reduced, and vice versa. In order to make sure that CorrF applies only to the class of interest it is multiplied by a classification image that corresponds to the spatial distribution of that land-cover class in the image. All other regions in the image which form the occurrence of all other classes are replaced with the value 1 and therefore have no effect on the original reflectance.

The resulting "selective CorrF" (CorrF') image is multiplied by the original reflectance image to remove its BRDF effects. The corrected value now reads

$$\rho'(\varphi_i, \theta_i\,;\, \varphi_r, \theta_N\,;\, \lambda) = \rho(\varphi_i, \theta_i\,;\, \varphi_r, \theta_r\,;\, \lambda) \cdot CorrF'(\varphi_i, \theta_i\,;\, \varphi_r, \theta_r\,;\, \lambda) \quad (6)$$

If an image is to be corrected for BRDF effects overall, this process has to be iterated for all land-cover classes that are contained within, using BRDF datasets from a goniometer for each class respectively. This requires a BRDF library of various materials at various illumination elevation angles. This labour-intensive work is worthwhile in the long run, assuming that BRDF datasets in the library will cover most common land-cover classes in a region of interest, and since they allow the user to correct imagery at which access is limited or even impossible.

DATA AND LOCATIONS

IGF data

The Israeli goniometric facility at the RSL-TAU, is designed to enable the manual positioning of a hand-held ASD FieldSpec Pro spectrometer and an illumination source, on a virtual hemisphere, at an angular resolution of 2.5° at both φ (azimuth) and θ (elevation) directions. It is constructed from two combined sliding arcs with a radius of 75cm and a base ring (see figure 2).

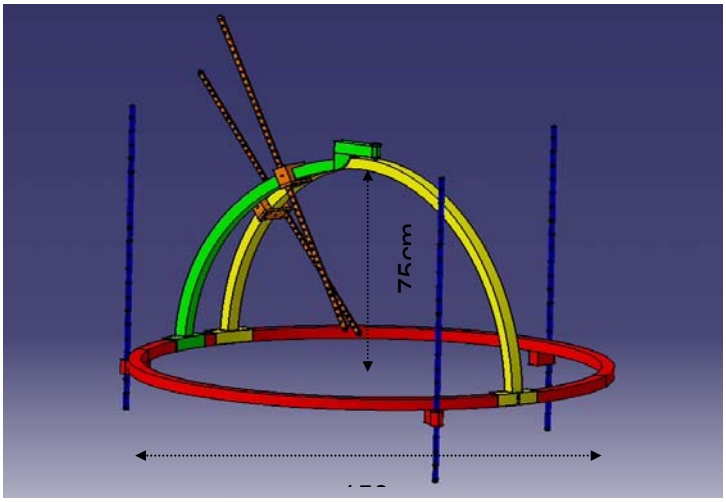

Figure 2. The Israeli Goniometric Facility (IGF) at the University of Tel-Aviv.

The IGF allows a mounted spectrometer to measure targets from a maximal distance of about 65cm (to hemisphere center-point). This results in a GIFOV of about 9cm across, from nadir, using an 8° fore optic. In this study we placed two fresh "Kikuyu" grass carpets (*Pennisetum Clandestinum*) side by side (covering 90x100cm in total) within the goniometer, and illuminated them with a stabilised diffuse light (standard ASD Lamp-Pro) from East (φ_i=90°). Three θ_i positions were used: 25°, 45° and 65°, covering most sun elevation angles of remotely sensed imagery.

In this study we used an 8° fore optic from a distance of 35cm. For each illumination position 113 radiance measurements (L) were taken on the hemisphere with a φ_r resolution of mostly 22.5° (45° interval only near Nadir, at θ_r angles of 70° and 80°) and a θ_r resolution of 10°. These radiance datasets were divided by perfect counterpart radiance datasets of a calibrated white reference (Spectralon®) plate of ASD, assumed to be Lambertian, such that for each sensor position we obtain a bi-directional reflectance factor (BRF). In order to facilitate the use of calculated anisotropy these measurements were projected to a Transverse Mercator (rectangular) projection, where 16 φ_r's and 9 θ_r's correspond to the sensor's angular φ_r and θ_r position respectively, and form the X

and Y dimensions of a model-image. Within this new layout data gaps at 70° and 80° θ positions are filled by inverse-distance interpolation and the nadir measurement is simply replicated 15 times for all nadir φ_r cells. Finally this dataset is interpolated to an artificially enhanced resolution of 5° in both directions.

HyMAP Data

Data were recorded on June 30th 2003 with the HyMAP sensor (viii), over Waging, Germany. The instrument consists of 4 spectrometers with 126 bands in total that cover the solar spectral region (except for the atmospheric water vapour region between 1.80-1.95µm) with a channel bandwidth between 10 and 15nm. 512 lines are measured at a FOV of approximately 61°. A flight altitude of roughly 2400m above ground level resulted in an average pixel size of 5m for the selected scenes. The flight heading, solar elevation and the solar azimuth for the different (sub)scenes used in this study are found in table 1. A subset of 303 columns x 283 lines was cut from all 4 images, corresponding to the same area, for convenience of comparison. All subsets contained nadir samples as well. Images were acquired between 08:30 and 10:30 UTC.

Table 1: Angles associated with HyMAP flights (degrees).

Flight line	Flight heading	Solar elevation (θ_l)	Solar azimuth (φ_l)
Waging01	118.91	41.8	101.7
Waging07	180.04	52.57	118.96
Waging13	89.98	59.43	136.2
Waging14	269.86	60.44	139.79

CASI data

Data were recorded on April 18th 1997 with the CASI sensor (ix), over Tel-Aviv, Israel. The selected instrument configuration consists of 48 bands in total that cover the VNIR spectral range (430-970nm) with a channel bandwidth between 6.1 and 6.3nm. 512 lines are measured at a FOV of 34.2°. A flight mean altitude of 1830m above ground level resulted in an average pixel size of about 4m in the selected scene. The mean flight heading was 259.95°, the solar elevation was 65.16° and the solar azimuth was 213.68° for the (sub)scene used in this study. A subset of 400 columns x 400 lines was cut around the Nadir column for convenience. The image was acquired at 10:30 UTC.

Spectral field measurements

Ground based reflectance measurements have been obtained at both locations with a handheld ASD FieldSpec Pro FR spectrometer. This spectrometer measures reflectance in a continuous spectrum from 350 to 2500nm at 1nm intervals. Reference spectra were taken of homogeneous highly reflective surfaces in order to validate sensor calibration and atmospheric correction, as well as for several grasslands with varying land use and physiological properties. All spectrometer measurements were taken at nadir view and converted to relative reflectance by dividing it by the reflected radiance from a Spectralon® reference panel, measured in the same geometric configuration.

Test sites

The HyMAP test site, Waging-Taching, is situated in the foreland of the Bavarian Alps at Lon 12° 45’ 51.33’’, Lat 47° 57’ 18.24’’, close to Salzburg. The selected test scenes cover nearly flat terrain. Land use at the test site is dominated by agriculture, of which around two thirds are constituted by grassland. Grassland use is predominantly intensive, and is represented by up to seven cuts a year, additional manuring of meadows, and frequent grazing (and the resulting constant dung input) in pastures. This might result in a grass/vegetation height ranging from 5cm to over 1m (The fields of different use and management intensity area are evenly scattered through the study area and range in size from the area of an average backyard to more than 25 hectares).

In contrast to that, the CASI test site is situated in the Northern part of the city of Tel-Aviv, Israel, at Lon 34° 50' 42'', Lat 32° 06' 25'', about 5km from the coast of the Mediterranean sea, in a flat terrain. It covers a mixed residential and commercial region around a large park area, along the Yarkon stream. Ground altitude is 5-10m above sea level. The dominant land use at this test site is the park itself, of which around two thirds are covered by grassland of type *Pennisetum Clandestinum* (commonly known as "Kikuyu" grass). This type of grass is typically short (~3-5cm) and rough.

METHODS

With the aim of extracting pixel-based correction factors, per wavelength, for a given real image, we put together 3 datasets: a scan-angle file, a BRDF dataset of the land-cover class to be treated, and a class map of the spatial occurrence of that land-cover class in the image. These are discussed here in more detail.

Radiometric and geometric corrections

For the direct georeferencing of the radiometrically calibrated HyMAP images a parametric approach was carried out. For the geocoding of the image the software program PARGE (vii) uses the flight attitude and DGPS position of the sensor recorded during the overflight, together with a digital elevation model of the area. Additionally a small number of ground control points (GCPs) was used, based on a 1:25000 topographical map of the area. CASI was radiometrically calibrated by dedicated software, and corrected for roll motion, but was left otherwise un-registered.

Atmospheric correction

The software tool ATCOR4 (x), based on the MODTRAN radiative transfer code was used for the combined correction of atmospheric and topographic effects of the wide field-of-view HyMAP imagery. Calibrated radiance data were converted to top of canopy reflectance using a few reference ASD ground spectra for in-flight calibration. In contrast to this, atmospheric correction of CASI data was not satisfactory, and therefore no atmospheric correction was used for the CASI data. Taking into account the flight heading and the sun's angular position at the time of acquisition we expected the asymmetry of the path-radiance to have a minor effect on the anisotropic behaviour of the surface itself.

BRDF correction

Three BRDF datasets of *Pennisetum Clandestinum* grass adjusted and resampled spectrally to each of the test images as discussed above. Radiance values were then converted to BRFs and further to ANIFs (figure 1). Finally ANIF values were inverted to form correction factors which were multiplied by the test images at those pixels that were classified as grass.

Test measures

The visual difference of BRDF correction is quite subtle to the eye. This is especially true if a single land-cover class is corrected, since the correction will apply only to those places where this class was identified by previous classification. Classification, as in many processing chains, is the weak link, and the extent of success depends substantially on correct classification results. In order to accentuate the effect of BRDF correction, all georeferenced HyMAP images were masked, leaving grass pixels only, then rotated with respect to the Nadir column so that it was up-oriented (from top to bottom of the image window). This orientation was already the case with the CASI image. Next, a sample of column based average ANIF values over all wavelengths were computed (every ~30 columns across each of the rotated images), and analysed with respect to wavelength values and to sensor elevation values θ_r. Additionally, NDVI values were calculated for all images before and after BRDF correction. These results are summarized and discussed in the following section.

RESULTS

A sample of mean column-based ANIF vectors of CASI before and after BRDF correction are illustrated in figure 3 (a,b) and show that anisotropy is indeed sensitive to wavelength as Sandmeier observed (vi). It also shows that the range of deviation of ANIF values decreased from about 0.4 in all bands to about 0.1 except the short-wave green (440nm) and red-edge (675nm) areas where a deviation of 0.2 was reached. This can be explained by the fact that at these spectral regions absorption is relatively strong, leaving less energy available for multiple scattering, resulting in higher anisotropy values. An additional interesting point is the fact that after correction some variability remains. This variation is expected, since natural vegetation variation does exist, as seen clearly in the original image (figure 1).

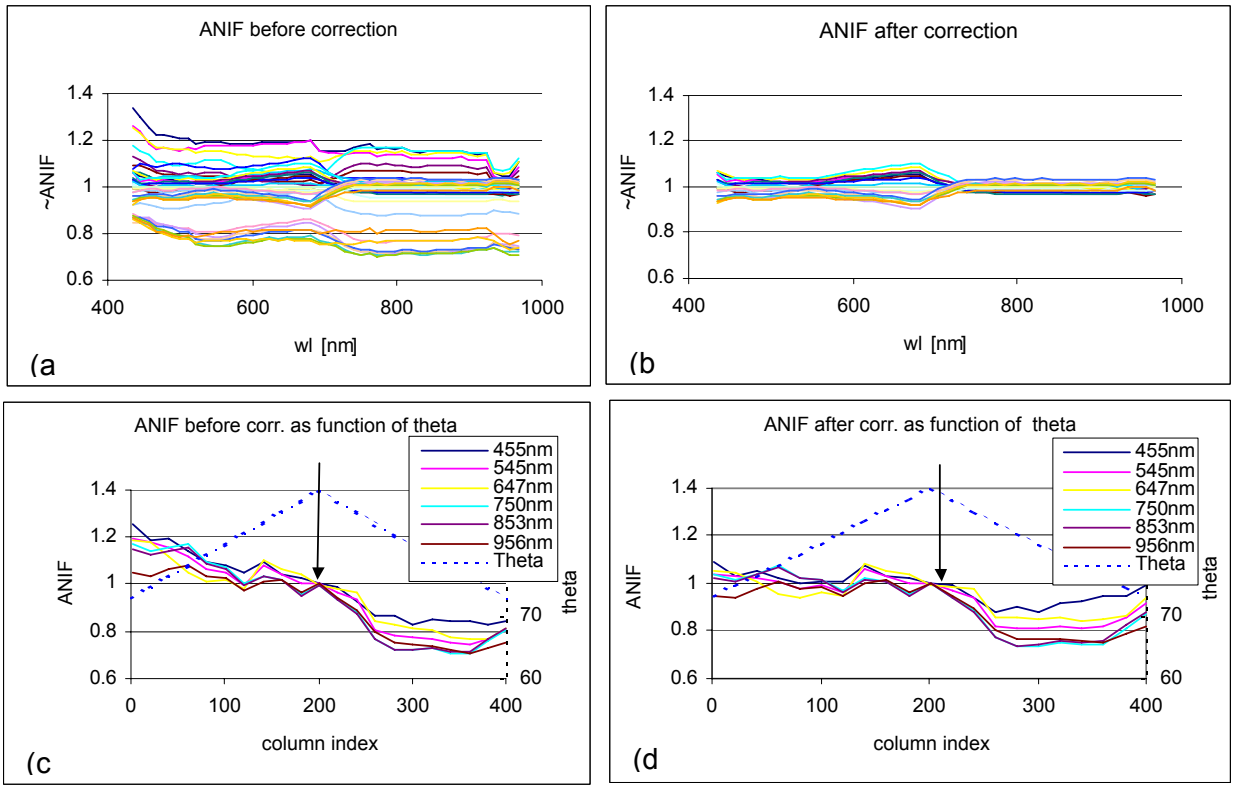

Figure 3. ANIF of CASI as function of wavelength, before (a) and after (b) correction, and as a function of sensor elevation angle θ_r before (c) and after (d) correction.

This emphasizes the fact that this type of correction, being based primarily on sensor and sun angles, leaves the spatial natural variability of land-cover classes unchanged. Figure 3 shows a cross-section of ANIF values for selected wavelengths across the Nadir column (i.e. orthogonal to the flight direction) before correction (Fig. 3c) and after it (Fig. 3d). The dashed lines represent the sensor elevation values (θ_r), and emphasize the unit ANIF at the nadir column. The overall "spectral rotation" of the image is clear from the ANIF vectors (Fig. 3c,d), and this rotation, although wavelength-specific, is consistent overall θ_r values.

The general trend of this behaviour can be expressed by an average vector of ANIF over the sample of wavelengths, as shown in figure 4(a). It can be seen that ANIF was most influenced by this correction at the edges of the image (further away from the nadir column) reaching about 13% difference at either side, and that this difference decreases gradually towards the center of the image. This trend is not always expected to be so clear since it depends primarily on the direction of the scan with respect to sun position.

Figure 4(b) presents the calculated root mean square error (RMSE) of ANIF values (with respect to unity) and shows that, in average, 85% of anisotropy of the grass were removed by this method at wavelengths where relatively high reflectance values occur. At spectral regions of relatively low

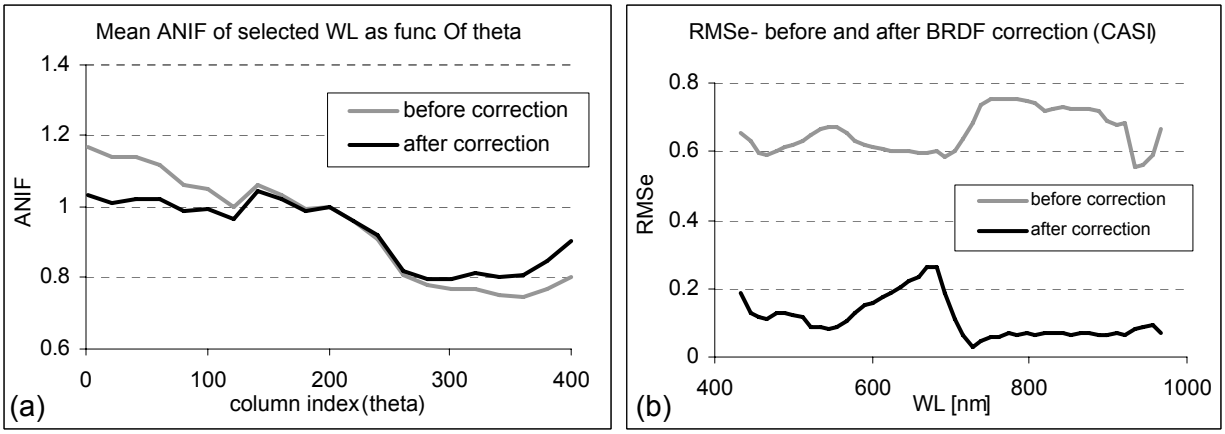

Figure 4. Measures of BRDF correction effectiveness in the CASI image: (a) average ANIF over some sample wavelengths (see figure 3c,d) and, (b) RMSE of the ANIF sample columns (see also figure 3a,b).

HyMAP data were corrected in the same way. The main difference in this case was the availability of scan-angle files with φ_r and θ_r bands related directly to in-flight navigation data. As an example, figure 5 shows the Waging test site and four resulting ANIF images (b-e). Here we limit the analysis of HyMAP results to the VNIR range only, as an example of the application of this correction method and for a more convenient comparison with CASI data. A sample of ANIF values from Waging 07 data are given in figure 6. The nadir column of this image is located at the right-most part of the image (see also figure 5c) and ANIF vectors consequently converge to unity.

Figure 5. A natural colour composite HyMAP image of the Waging test site (a), and resulting ANIF images (λ=0.859μm): Waging01 (b), Waging07 (c), Waging13 (d), Waging14 (e). The change from bright to dark in ANIF values corresponds to the varying flight directions, and represents nadir lines.

Results of applying the correction method to this dataset are illustrated in figure 6. Assessing ANIF before and after correction, it is clear that performance is reduced with comparison to CASI data (see figure 3) for possible reasons discussed below.

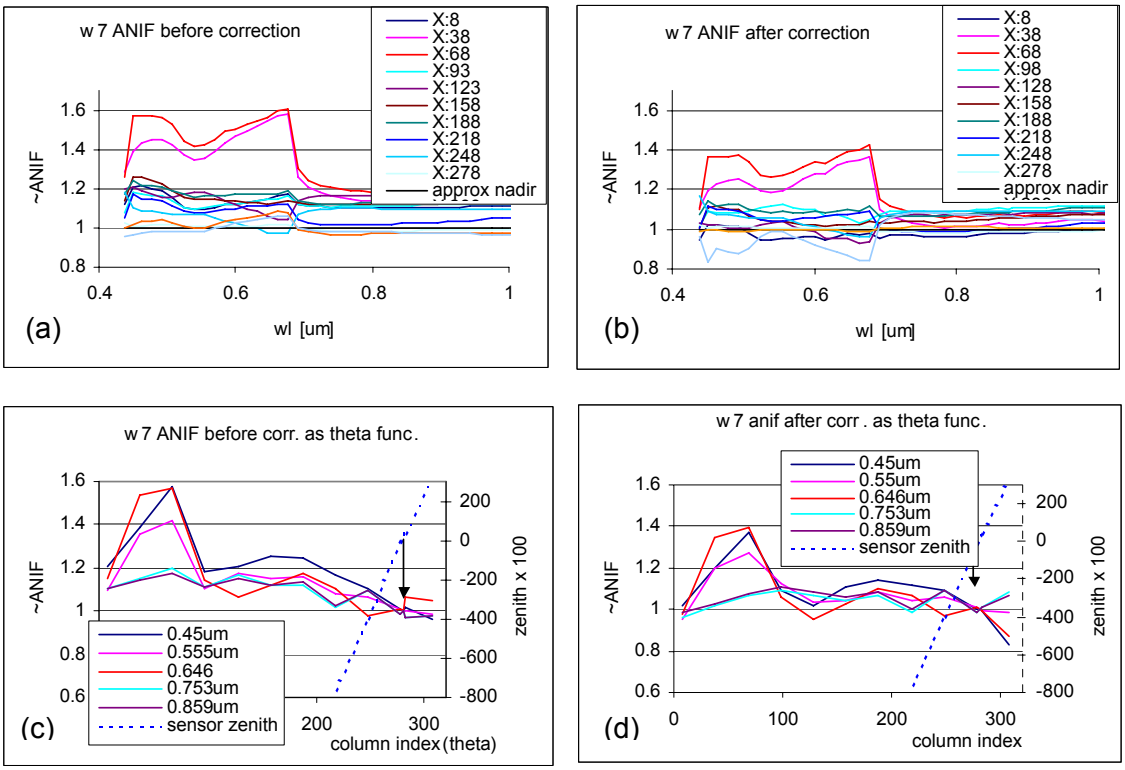

Figure 6. Column-based mean ANIF vectors of grass for the Waging07 dataset. Values as function of wavelength (a,b) and as a function of sensor zenith angle (c, d).

In figure 6a and 6b we see between 0.7-1.0μm some 50% decrease in anisotropy (ANIF difference of ~0.1). ANIF is less affected in the visible range. With respect to sensor zenith angles before correction (Fig.6c) and after it (Fig.6d) a slight improvement for all sample wavelengths, and a general trend of nadir-normalization is observed. As expected, the correction effect is most influential farthest from the nadir line.

One especially interesting result is probably the comparison of calculated outputs of the various HyMAP datasets, covering the same region from different flight directions. In order to have a notion of the effect of BRDF correction, NDVI values were computed for the four HyMAP images before and after correction within areas where all their corresponding classification results agreed. Their respective global means and standard deviations were also compared. With respect to HyMAP spectral sampling we defined NDVI as

$$NDVI=(0.859\mu m-0.662\mu m)/\ (0.859\mu m+0.662\mu m) \qquad (7)$$

A summary of the NDVI comparison is given in figure 7. Waging01, waging07 and waging13 datasets show a minor change after correction compared to pre-correction mean NDVI values. The Waging14 dataset shows a larger change of values. Overall, mean values change by less than 1%, except Waging14 which changes by almost 3%. The overall standard deviation of all mean NDVI values together, doubled after correction.

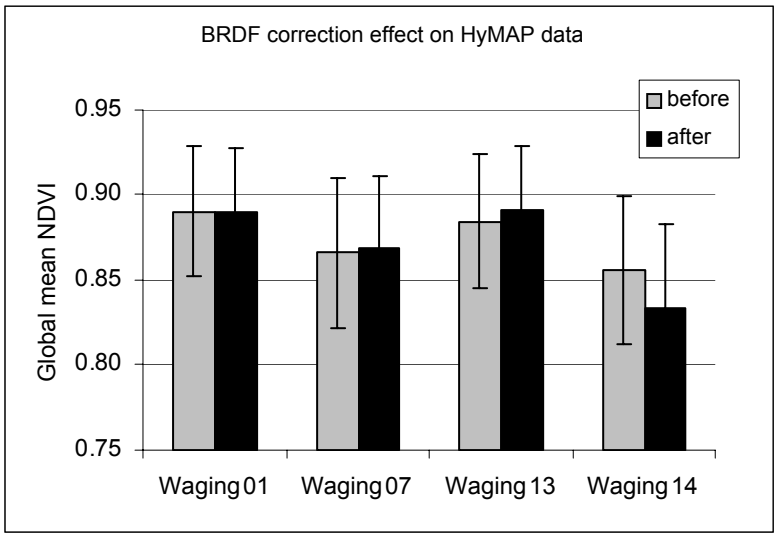

Figure 7. NDVI values for 4 HyMAP datasets, before and after BRDF correction.

DISCUSSION

Testing this method on a CASI non-georeferenced image from Tel-Aviv, up to 85% improvement was achieved. When applied to HyMAP georeferenced images from Waging, Germany, a 50% improvement was achieved at the visible range. An overall comparison of global NDVI mean values proved that this method is sensitive to the application of a correct BRDF dataset, when vegetation is applied. The performance of correction to HyMAP data may be explained by several error factors. The first is that the setup of the IGF measuring grass was such that the GIFOV of the spectrometer could be non- representing of anisotropic behaviour of larger patches of such grass. The second could be the result of varying phenological states, or different grass types with varying structure and related anisotropic characteristics. Finally, the illumination of the IGF, although diffuse within its own beam, is directional, while natural illumination is hemispherical. This results in different shadowing effects than in the field and to slightly different anisotropic behaviour.

SUMMARY & CONCLUSION

This paper presents a new empirical BRDF correction method, which is entirely based on laboratory BRDF measurements, assuming that the measured materials are found in the image to be corrected. We combine primarily sensor scan angle information from flight navigation data, BRDF datasets from the Israeli Goniometric Facility (IGF) and classification data, to generate a vector of anisotropy factors (ANIF), per pixel, and corresponding correction factors. In this study, BRDFs were collected for *Pennisetum Clandestinum* grass that is commonly growing in Israel in recreation parks. We prove that BRDF can be corrected using laboratory measurements of anisotropy. Although this is a labour-intensive correction method, it is based on a high-resolution spectral and angular sampling strategy and may be valuable if access to a region of interest for in-situ measurements is difficult or if image-based samples are not enough for such a correction. Further we show that the decrease of anisotropy in a corrected image is wavelength-sensitive and performs best (in the case of vegetation) at wavelengths where reflectance is relatively high (i.e. at the green and NIR spectral ranges). Finally it is clear that performance of this correction depends primarily on the availability of materials existing in the scene itself, for laboratory measurements. With growing interest in BRDF, such corrections are expected to become a routine link in pre-processing, along with radiometric, atmospheric and geometric corrections.

ACKNOWLEDGEMENTS

We would like to thank the DAAD program (Germany) and the SAPIR fund of the PAIS foundation (Israel) for their support in this research. We would also like to thank Prof. Juval Portugali from the University of Tel-Aviv for his support in the making of the IGF and Mrs. Lee Sever who assisted in measuring with the IGF.

References

i Beisl U, 2001. Correction of Bidirectional Effects in Imaging Spectrometer Data, PhD Thesis, Remote Sensing Series 37, RSL, University of Zurich, 189 pp.

ii Roujean J, M Leroy and P Deschamps 1992. A bidirectional reflectance model of the earth's surface for correction of remote sensing data, J. of Geoph. Res., 97(D18):20455–20468

iii Cierniewski J and A Karnieli, 2003. Virtual surfaces simulating the bidirectional reflectance of semiarid soils. Int. J. Remote Sensing, 24(7): 1469–1486

iv Richter R, 2005. Atmospheric / Topographic Correction for Airborne Imagery, DLR report DLR-IB 565-02/05, Wessling, Germany

v Nicodemus F E, J C Richmond, J J Hsia, I W Ginsberg and T Limperis, 1977. Geometrical considerations and nomenclature for reflectance, Nat. Bur. Standards Mono., 160(52)

vi Sandmeier S, C Müller, B Hosgood and G Andreoli, 1998. "Physical Mechanisms in Hyperspectral BRDF Data of Grass and Watercress, Remote Sensing of Environment, 66(2): 222-233

vii Schläpfer D, M Schaepman, and K Itten, 1998. PARGE: Parametric Geocoding Based on GCP- Calibrated Auxiliary Data. In: SPIE Int. Symp. on Opt. Sc, Eng. and Instr., San Diego (CA), 334 – 344

viii Cocks T, R Jenssen, A Stewart, I Wilson and T Shields, 1998. The HyMap™ airborne hyperspectral sensor: the system, calibration and performance. In: 1st EARSeL Workshop on Imaging Spectroscopy, (EARSeL, Zurich), 37-42

ix Ben-Dor E, N Levin and H Saaroni 1998. Utilization of imaging spectroscopy in urban areas: A case study over Tel-Aviv, Israel using the CASI sensor. In: 1st EARSeL Workshop on Imaging Spectroscopy, (EARSeL, Zurich), 473-479

x Richter R, 2002. Atmospheric / Topographic Correction for Wide FOV Airborne Imagery: Model ATCOR4, Report DLR-IB 552-05/99, Wessling, Germany